

Is the North Atlantic Oscillation a Breaking Wave?

CHRISTIAN FRANZKE*

EMS Environment Institute, The Pennsylvania State University, University Park, Pennsylvania

SUKYOUNG LEE

Department of Meteorology, The Pennsylvania State University, University Park, Pennsylvania

STEVEN B. FELDSTEIN

EMS Environment Institute, The Pennsylvania State University, University Park, Pennsylvania

(Manuscript received 4 December 2002, in final form 1 August 2003)

ABSTRACT

Given the recent observational evidence that the positive (negative) phase of the North Atlantic Oscillation (NAO) is the remnant of anticyclonic (cyclonic) wave breaking, this study uses a multilevel primitive equation model to investigate important dynamical attributes of the above wave breaking behavior. For this purpose, a hierarchy of different basic states (two- and three-dimensional) and initial perturbations are used.

With the three-dimensional climatological flow as the basic state, it is found that initial perturbations located equatorward (poleward) and upstream of the climatological Atlantic jet lead to wave breaking similar to that of the positive (negative) NAO phase. Consistently, analysis of observational data indeed shows that the Pacific storm track is displaced equatorward (poleward) prior the onset of the positive (negative) NAO phase. This result suggests that the latitudinal position of the Pacific storm track plays an important role for determining the phase of the NAO. Sensitivity experiments show that individual life cycles resemble each other only within the NAO region, but have large case-to-case variability outside of the NAO region.

Calculations with zonally symmetric basic states fail to produce wave breaking of the correct spatial and temporal scale, underscoring the dynamical significance of the three-dimensional climatological flow.

1. Introduction

The atmospheric flow of the Atlantic sector and surrounding continents exhibits considerable variability on a wide range of time scales. The North Atlantic Oscillation (NAO; Defant 1924; Walker and Bliss 1932; Bjerknes 1964) is the dominant mode of winter low-frequency variability in the North Atlantic region, ranging from central North America to Europe and even into northern Asia and the Middle East. The NAO is associated with changes in the location of storm tracks, regional anomalies in precipitation and temperature (Hurrell 1995), large-scale sea surface temperature anomalies (SST), and also has an impact on the flora and fauna (Marshall et al. 2001; Walther et al. 2002).

The fundamental mechanisms determining the evolution of the NAO are, however, still far from being understood. It is not clear whether the NAO is simply due to driving by stochastic weather events, or whether ocean dynamics in the North Atlantic Ocean, coupling with the stratosphere or interaction with other climate subsystems play an active role in controlling the evolution of the NAO (Marshall et al. 2001 and references therein).

In a study by Feldstein (2003), it is shown that the NAO undergoes a complete life cycle of growth and decay within a time period of about 2 weeks. The same time scale has been shown to exist in an idealized modeling study for a NAO-like anomaly (Franzke et al. 2001). Furthermore, Feldstein (2003) shows that the NAO is driven by both high-frequency (periods < 10 days) and low-frequency (periods > 10 days) transient eddy vorticity fluxes. These results suggest that intra-seasonal time-scale processes are fundamental to the NAO, although other processes involving the ocean and stratosphere can be important.

While the above relatively short time scales and processes indicate that the NAO is associated with transient

* Current affiliation: Courant Institute of Mathematical Sciences, Center for Atmosphere–Ocean Science, New York University, New York, New York.

Corresponding author address: Dr. Christian Franzke, Courant Institute of Mathematical Sciences, New York University, 251 Mercer St., New York, NY 10012.
E-mail: franzke@cims.nyu.edu

waves, it is unclear how the physical processes involved with these waves affect the evolution of the NAO. Benedict et al. (2004, BLF hereafter) show that the two NAO phases arise from two different types of wave breaking. By investigating potential temperature on the nominal tropopause, they show that the wave undergoes anticyclonic¹ breaking during the positive NAO phase. For the negative phase, the wave breaks cyclonically.² It is the breaking waves themselves that BLF suggest is the NAO anomaly. In another study, Lee and Feldstein (1996) also find that these two distinct types of wave breaking exist within baroclinic wave packets in an aquaplanet GCM.

To put the results of BLF in a broader perspective, we consider three important concepts for low-frequency variability. The first sees planetary-scale instabilities as the origin of low-frequency variability (Frederiksen 1983; Simmons et al. 1983); the second interprets low-frequency variability as arising from the interaction among synoptic-scale transients (Vautard and Legras 1988; Cai and Mak 1990; Lau and Nath 1991; Robinson 1991). The third view sees low-frequency variability as remotely forced stationary waves (Hoskins and Karoly 1981; Trenberth et al. 1998). The first concept is not inconsistent with the finding that the Pacific–North American (PNA) pattern can be understood as a *linear* initial-value problem (Cash and Lee 2001; Feldstein 2002). The results to be presented in this study reveal that the NAO can also be viewed as an initial-value problem, but that the NAO is fundamentally different from the PNA in that *nonlinear* wave breaking is crucial for the NAO. These findings suggest that the second concept is also highly relevant for the NAO. The third concept can be viewed as a boundary-value problem. Given the relatively short time scale of the PNA and NAO, as discussed above, it is likely that these boundary processes primarily act to modulate the PNA and NAO on time scales longer than that of the life cycle of these teleconnection patterns.

The study of BLF raises the question as to whether NAO evolution can be thought of as a nonlinear initial-value problem, with the initial perturbation beginning as a synoptic-scale wave. If so, the natural question to ask is: what are the important features that control the sense of wave breaking and, therefore, the NAO phase? This study addresses these questions by investigating the NAO evolution as a nonlinear initial-value problem. For this purpose, we perform baroclinic life cycle experiments with a multilevel primitive equation model. The zonally symmetric and asymmetric basic states are derived from the National Centers for Environment Pre-

dition–National Center for Atmospheric Research (NCEP–NCAR) reanalysis data, with both normal modes and localized finite amplitude perturbations as initial disturbances. In a manner consistent with BLF, we will see that both phases of the NAO are associated with a distinct type of wave breaking.

Section 2 gives a description of the model and the datasets. Observational evidence is presented in section 3, followed by the results of the experiments with a three-dimensional basic state in section 4, and a zonally symmetric basic state in section 5. The conclusions are given in section 6.

2. Model description and data

a. Model

For this study, we use a spectral sigma-level primitive equation model developed at the Geophysical Fluid Dynamics Laboratory (GFDL; Held and Suarez 1994; Feldstein 1994; Kim and Lee 2001a,b). It consists of the dynamical core of a general circulation model. The horizontal resolution is truncated at rhomboidal 30 (R30), and there are 14 vertical sigma levels. The only physical parameterization included is an eighth-order hyperdiffusion, which accounts for enstrophy cascade to unresolved scales. Furthermore, three additional sets of experiments with surface friction included have been carried out. These experiments have a surface friction damping time scale at the lowest sigma level of $\frac{1}{2}$, 1, and 2 days. See Held and Suarez (1994) for a detailed description of the surface friction scheme.

b. Data

The daily (0000 UTC) NCEP–NCAR surface pressure, vorticity, divergence and temperature fields on 14 reanalysis model sigma levels are used together with the 300-hPa streamfunction field. The latter quantity is obtained by logarithmic linear interpolation. These data cover the years 1958 to 1997 for the months of November through March. The seasonal cycle is removed at each grid point. The seasonal cycle is obtained by taking the calendar mean for each day and applying a 20-day low-pass digital filter. All data used in this analysis are truncated at rhomboidal 30 resolution. For all simulations, the flow is assumed to be symmetric across the equator; that is, the Northern Hemisphere (NH) data are mirrored and used in the Southern Hemisphere (SH).

c. Basic states

Two classes of basic flows are used in this study. One is a zonally varying three-dimensional flow, and the other is zonally symmetric. For the zonally varying basic state, we consider three cases: the NH three-dimensional wintertime mean flow, and the three-dimensional positive and negative phases of the NAO. For the latter

¹ Anticyclonic wave breaking is characterized by backward-tilted, thinning troughs with SW–NE tilt, which are advected anticyclonically on the equatorward side of the jet (Thorncroft et al. 1993).

² Cyclonic wave breaking is described by forward-tilted troughs with SE–NW tilt wrapping themselves up cyclonically on the poleward side of the jet (Thorncroft et al. 1993).

two cases, the basic state is specified as the composite flow prior to the onset of the NAO. The zonally symmetric basic states, to be discussed in section 5, are derived by taking partial zonal averages of the climatological flow over the following domains: 120°–60°W, 130°–80°W, 80°–30°W, 60°W–0°, 90°W–0°. Three cases are again considered: the climatological flow, and the positive and negative phases of the NAO.

The numerical study of the growth of unstable initial disturbances requires an initial basic flow that by itself is a steady solution of the model's equations (Hoskins and Simmons 1975; Branscome et al. 1989; Feldstein 1994). To derive a steady zonally symmetric basic state, we first set the meridional and vertical velocities equal to zero. The only nonzero fields are temperature, zonal wind, and surface pressure. These conditions lead to the vanishing of all time tendencies except for that of the divergence. The requirement that the divergence tendency also vanish gives a balance condition for the mass and momentum fields that ensures steady flow (Branscome et al. 1989). The nonlinear balance condition is then iteratively solved for the zonal wind. To obtain the nonlinear balanced basic state, the observed partial zonally averaged surface pressure is reduced to sea level pressure to account for the effect of orography. Because this changes the sigma levels, the temperature field is then linearly interpolated to the new sigma levels. Then, the geopotential height is calculated from the temperature field.

In order to obtain a steady basic state from the three-dimensional winter climatological flow we have to specify a forcing term \mathbf{F}_A (e.g., James et al. 1994). In general, the climatological mean flow $\bar{\mathbf{X}}^c$ is not a balanced state:

$$\frac{\partial \bar{\mathbf{X}}^c}{\partial t} = \mathbf{L}(\bar{\mathbf{X}}^c) + \mathcal{N}(\bar{\mathbf{X}}^c, \bar{\mathbf{X}}^c) \neq 0, \quad (1)$$

where \mathbf{L} is a linear operator, and \mathcal{N} represents nonlinear processes. Therefore, we have to add a forcing term \mathbf{F}_A to (1) to ensure a steady state:

$$\frac{\partial \bar{\mathbf{X}}^c}{\partial t} = \mathbf{L}(\bar{\mathbf{X}}^c) + \mathcal{N}(\bar{\mathbf{X}}^c, \bar{\mathbf{X}}^c) + \mathbf{F}_A = 0. \quad (2)$$

This is accomplished by first integrating $\partial \mathbf{X}/\partial t = \mathbf{L}(\mathbf{X}) + \mathcal{N}(\mathbf{X}, \mathbf{X})$ one time step forward with $\bar{\mathbf{X}}^c$ as the initial state. The quantity \mathbf{F}_A in (2) is then specified to be equal to $\partial \mathbf{X}/\partial t$ from this one time step integration. The model equations can then be written as

$$\frac{\partial \mathbf{X}}{\partial t} = \mathbf{L}(\mathbf{X}) + \mathcal{N}(\mathbf{X}, \mathbf{X}) + \mathbf{F}_A. \quad (3)$$

By subtracting (2) from (3) we get

$$\frac{\partial \mathbf{X}}{\partial t} = \mathbf{L}(\mathbf{X}) - \mathbf{L}(\bar{\mathbf{X}}^c) + \mathcal{N}(\mathbf{X}, \mathbf{X}) - \mathcal{N}(\bar{\mathbf{X}}^c, \bar{\mathbf{X}}^c). \quad (4)$$

The corresponding symbolic form for the primitive

equations, which would not include the additional forcing term \mathbf{F}_A , is

$$\frac{\partial \mathbf{X}}{\partial t} = \mathbf{L}(\mathbf{X}) - \mathbf{L}(\bar{\mathbf{X}}^c) + \mathcal{N}(\mathbf{X}, \mathbf{X}) - \mathcal{N}(\bar{\mathbf{X}}^c, \bar{\mathbf{X}}^c) - \overline{\mathcal{N}(\mathbf{X}', \mathbf{X}')^c}. \quad (5)$$

By comparing (4) with (5), it can be seen that the requirement for the observed climatological flow to be a steady solution to (1) implies that there is an extra term $\overline{\mathcal{N}(\mathbf{X}', \mathbf{X}')^c}$ in the model equations. Since the quantity $\mathcal{N}(\mathbf{X}', \mathbf{X}')^c$ is independent of time, we can crudely estimate that $\mathcal{N}(\mathbf{X}', \mathbf{X}')^c$ has an important influence after a time period of $\tau = |\mathbf{X}'|/|\mathcal{N}(\mathbf{X}', \mathbf{X}')^c|$. We estimate τ by using the anomalous streamfunction from the model integrations for \mathbf{X}' , and the observed, climatological, inverse Laplacian of the transient eddy vorticity flux divergence for $\mathcal{N}(\mathbf{X}', \mathbf{X}')^c$. The results indicate a value for τ of 20 to 30 days near the northern center of the NAO dipole and 10 to 15 days near the southern center of the NAO dipole. As the model integrations in this study are typically of a length near 10 days, these values for τ suggest that the impact of $\mathcal{N}(\mathbf{X}', \mathbf{X}')^c$ is unlikely to be large. This relatively small role played by $\mathcal{N}(\mathbf{X}', \mathbf{X}')^c$ is borne out in the model integrations, which, as we will see, find many similarities with the observed NAO life cycle.

d. Initial perturbations

The localized finite amplitude perturbations are derived from 40 yr of NCEP–NCAR reanalysis data by using the regression of high-pass-filtered (periods less than 10 days) surface pressure, divergence, vorticity and temperature on all sigma levels against the 300-hPa streamfunction at various grid points. These grid points are zonal direction 30°E, 0°, 30°W, 60°W, 90°W, 120°W, 150°W, 180°, and 210°W with higher resolution at every 3.25° longitude between 120° and 150°W, and meridional direction between 26° and 70°N at each grid point of the Gaussian grid. Figure 1 shows two selected initial disturbances for base points at 30°N, 150°W and 60°N, 150°W. These initial perturbations represent baroclinic wave trains. Furthermore, normal mode disturbances will also be used as initial disturbances.

e. Methodology

We examine potential temperature θ on a constant potential vorticity (PV) surface defined by $PV = 2$ potential vorticity units (PVU), where $PVU = 10^{-6} \text{ m}^2 \text{ s}^{-1} \text{ K kg}^{-1}$. As the 2-PVU surface is located within the tropopause, an examination of θ on this surface can clearly illustrate the dynamical processes taking place. The potential vorticity is calculated on the 14 sigma levels. The θ value on the 2-PVU surface is found by linear interpolation starting from the uppermost sigma level. An extensive review of PV– θ concepts and their

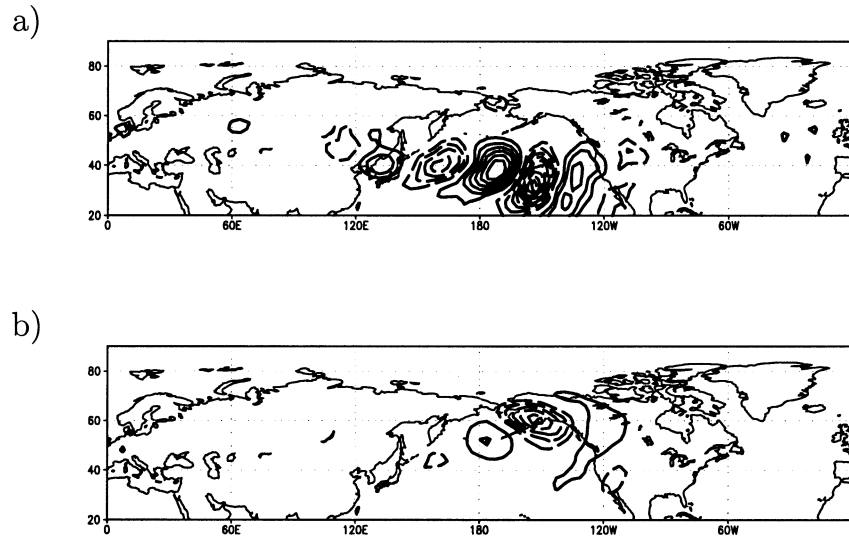


FIG. 1. High-pass-filtered (periods < 10 days) initial perturbation vorticity on $\sigma = 0.258$ for the base points at (a) 30°N , 150°W and (b) 60°N , 150°W . Contour interval is $1 \times 10^{-6} \text{ s}^{-1}$.

relevance to cyclone behavior is given by Hoskins et al. (1985).

The positive phase of the NAO is defined to begin when its principal component time series (obtained from Feldstein 2003) first exceeds one standard deviation and exceeds this value for at least five consecutive days. The negative phase is defined in an analogous manner. Composites are derived either by centering them around the onset day defined to be the first day of an NAO phase or around the maximum (minimum) of a positive (negative) NAO phase.

3. Observational evidence

As a reference for the model calculations, it is useful to first examine composites centered around the maximum (minimum) of the observed potential temperature on the 2-PVU surface for the positive (negative) NAO phases (Fig. 2). Also, for comparison, the climatological potential temperature field on the 2-PVU surface is illustrated in Fig. 3. For the positive phase (Fig. 2a), extending across the North Atlantic between Florida and Great Britain, the potential temperature field shows the typical characteristics of anticyclonic wave breaking. In this region, one can see disturbances with a strong SW–NE tilt. Furthermore, a secondary region of weaker anticyclonic wave breaking is present off the west coast of the southern United States and Mexico. In contrast, for the negative NAO phase (Fig. 2b), cyclonic wave breaking with a strong SE–NW tilt is present over the middle- and high-latitude North Atlantic. We verify that these two types of wave breaking are indeed associated with the two NAO phases by showing that the anomalous (deviation from the climatological value) 300-hPa streamfunction field (Fig. 2c for the positive phase, and

Fig. 2d for the negative phase) exhibits the familiar dipole pattern in the North Atlantic.

Since a calculation of the anomalous potential temperature field for either NAO phase is found to yield similar spatial patterns, but of opposite sign, we illustrate just the difference in the potential temperature field between the two phases (positive minus negative phase; see Fig. 2e). As can be seen, this spatial pattern is very similar to that of the anomalous streamfunction field for both phases (Figs. 2c and 2d). An examination of the anomalous potential temperature field allows us to relate the wave breaking processes shown in Figs. 2a and 2b to the dipole patterns in Figs. 2c, 2d, and 2e. First, for the positive NAO phase, we can understand that the southern anomaly in the dipole arises from poleward warm advection associated with the anticyclonic wave breaking over the Atlantic. For the northern anomaly in this dipole, it can be seen to arise from a southeastward cold advection. As discussed in section 4, and also in BLF, this cold advection is associated with the anticyclonic wave breaking off the west coast of the southern United States and Mexico. With regard to the negative NAO phase, the picture appears to be simpler, as it is northwestward warm advection that accounts for the northern anomaly and southeastward cold advection for the southern anomaly. This warm and cold advection are both taking place within the same cyclonically breaking wave.

Another starting point of this study is to consider the possible influence of the Pacific storm track for triggering NAO events. Chang (1993) gives evidence that some wave trains emanating from Asia propagate over the North American continent into the Atlantic. Similar results have been found by Higgins and Schubert (1993). A study of observed cyclone activity by Sickmüller et

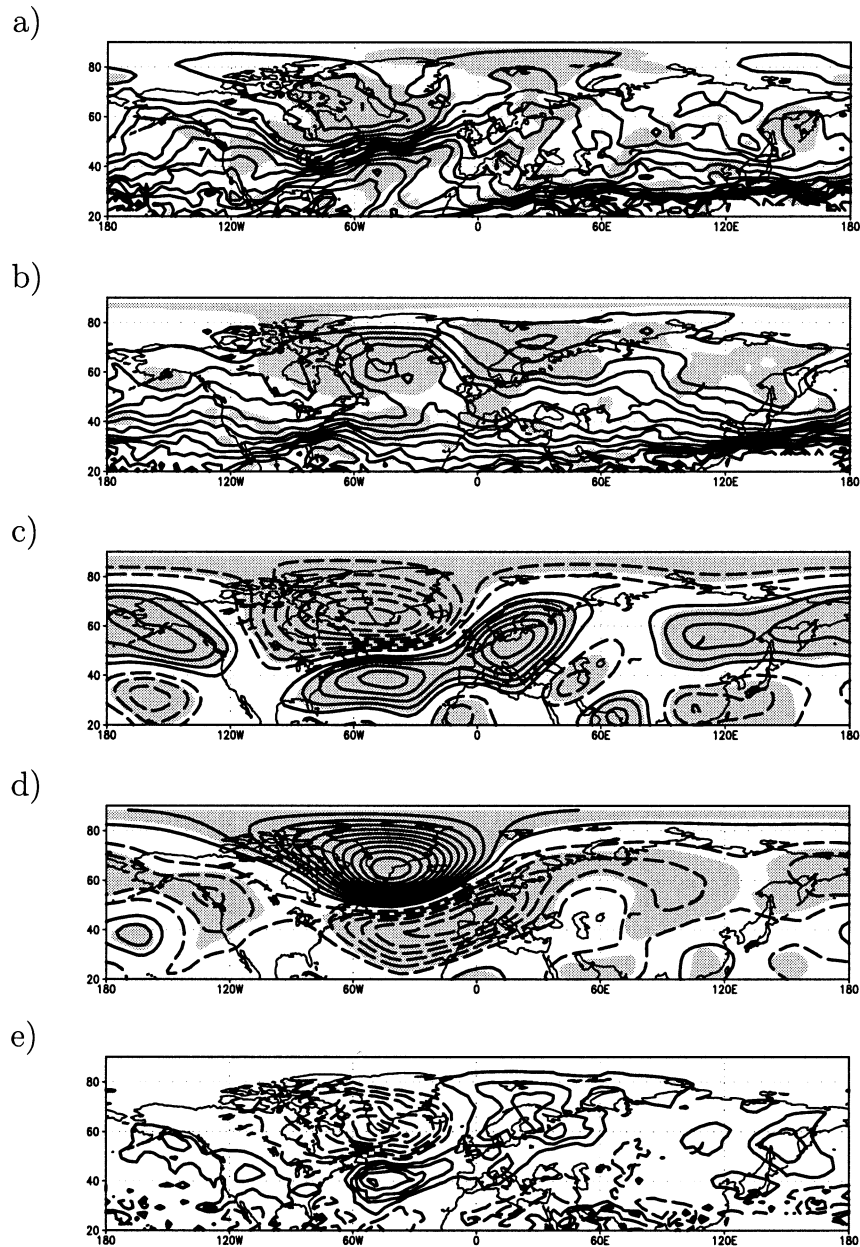


FIG. 2. NAO composites: potential temperature on the 2-PVU surface for the (a) positive phase (25 cases) and (b) negative phase (26 cases); 300-hPa anomalous streamfunction for the (c) positive phase and (d) negative phase; (e) difference between the potential temperature on the 2-PVU surface of the positive and negative phases. Contour interval is 5.0 K for the potential temperature and $2 \times 10^6 \text{ m}^2 \text{ s}^{-1}$ for the streamfunction, and shading indicates values that exceed the 95% significance level of a Student's t test.

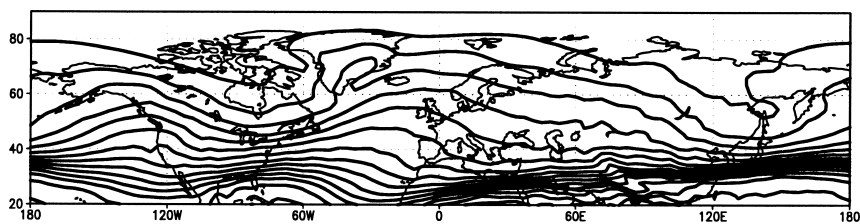


FIG. 3. Climatological potential temperature on the 2-PVU surface (contour interval is 5.0 K).

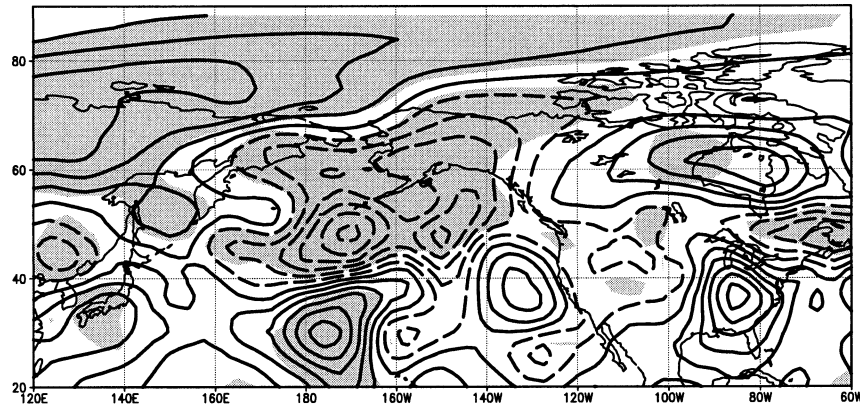


FIG. 4. 300-hPa high-pass-filtered streamfunction variance averaged over days -5 to 0 : difference between the positive and negative phase of the NAO (contour interval is $1 \times 10^{13} \text{ m}^2 \text{ s}^{-1}$; shading indicates values that exceed the 95% significance level of a Student's t test).

al. (2000) gives further evidence for this possible link between the two ocean basins.

Because it takes a few days for these upstream storm track eddies to reach the NAO region, we examine storm tracks averaged over 5 days before the onset of either phase of the NAO. In Fig. 4, we show the difference between the positive and the negative streamfunction variance composites. This calculation indicates that the Pacific storm track is shifted equatorward (poleward) prior to the onset of the positive (negative) NAO phase between 160°E – 140°W . This result suggests that meridional fluctuations in the latitude of the Pacific storm track may play a role for triggering the NAO.

4. Three-dimensional climatological basic state

a. Control cases

To see if it is possible to treat the temporal evolution of the NAO as a nonlinear initial-value problem, the three-dimensional climatological winter (November through March) flow (Fig. 3) is used as a basic state for life cycle calculations. High-pass-filtered regression patterns of observational data are used as baroclinic initial perturbations (see section 2d). Since these finite-amplitude perturbations are derived by regressing all model variables onto the 300-hPa streamfunction time series at different base points, these perturbations represent climatological synoptic-scale waves and contain no a priori information about the NAO.

Figure 5 shows the evolution of θ on the 2-PVU surface for the base point of the initial perturbation at 30°N , 150°W . For these calculations, day 0 corresponds to the flow at the beginning of the model run, and the other day numbers indicate the amount of time that has elapsed since the start of the model integration. (These definitions imply that day 0 of the model integration roughly corresponds to several days before the onset of the observed NAO.) A hint of a wave breaking can be discerned by examining the evolution of the sixth con-

tour from the top of the figure. At day 3 (Fig. 5a), a pronounced NE–SW tilt can be seen along the west coast of North America. By day 5, the northeastward excursion of this contour results in a kink in its structure over Montana. By day 7, this kink disappears. Such behavior is consistent with weak anticyclonic wave breaking followed by mixing, and is also consistent with the observations shown in BLF. This results in the advection of warm air into the Gulf of Alaska, and the advection of cold air into the southwest United States. Two days later (Fig. 5b), the primary changes are that the cold air associated with the anticyclonic wave breaking is advected eastward toward the center of the North American continent. By day 7 (Fig. 5c), the cold air has reached the northwest Atlantic, and anticyclonic wave breaking has started to take place to the southeast in the central North Atlantic. This anticyclonic wave breaking continues to amplify through days 9 and 10 (Figs. 5d,e). This results in the advection of warm air that extends northeastward toward Great Britain and the advection of cold air equatorward over the east coast of North America and over Greenland. The decay of this wave is apparent on day 11 (Fig. 5f). As can be seen, by comparing Fig. 5f with the climatological flow in Fig. 2, the northwestward displacement of the warm tropical air is much greater than the southwestward movement of the colder midlatitude air. These differences account for why the North Atlantic wave breaking is dominated by a positive anomaly.

The anticyclonic breaking wave in the North Atlantic, shown in Fig. 5, occurs at about the same location as in the observed composite field (Fig. 2a) and has the same tilt as the positive NAO phase. Its spatial scale is also in good agreement with the observed breaking wave (BLF). As will be discussed in section 4b, the anomaly field corresponding to Fig. 5 indicates a typical NAO dipole pattern in the North Atlantic. Taken together, the results suggest that the two centers of the dipole for the positive NAO phase arise from *two* wave breaking

events. The higher-latitude negative center appears to be due to the eastward advection of cold air that is a remnant of the anticyclonic wave breaking along the North American west coast (Fig. 5a). The lower-latitude positive center appears to be a remnant of the anticyclonic wave breaking over the North Atlantic. Since the wave breaking along the North American west coast is followed by the development of a downstream wave that subsequently breaks over the North Atlantic, these two wave breakings appear to be linked through downstream development as Rossby wave dispersion in an eastward direction takes place. This picture is consistent with the morphology sketched by BLF (see Fig. 7 of their paper).

The temporal evolution of θ on the 2-PVU surface with the base point of the initial perturbation located farther north at 60°N, 150°W is shown in Fig. 6 for day 3 and for days 6 through 9. As can be seen at day 3 (Fig. 6a), unlike for the above example with the base point at 30°N, 150°W there is little wave development upstream of the NAO region. As the wave over the North Atlantic grows (Figs. 6b–e), high- θ air is advected northwestward over Greenland, and low- θ air is advected southeastward. This results in anomalously warm air over Greenland and anomalously cold air over the North Atlantic, as in Fig. 2c for the negative phase of the NAO. The evolution of θ shows the same tilt of the breaking wave as for the negative NAO phase. The location and spatial scale are again in good agreement with the observed NAO composite for the negative phase.

The low-frequency (period greater than 10 days) evolution of the NAO was also examined by Feldstein (2003). He reports the occurrence of an anomalous low-frequency wave train that propagates across the North Pacific toward the east coast of North America prior to the formation of the positive NAO phase. This contrasts the negative NAO phase, where the low-frequency development was found to be in situ. The low-frequency wave train in the positive NAO phase is composed of several centers, including a negative center over the northwestern United States and southwestern Canada. Although not evaluated in this study, as BLF show, it is plausible that this low-frequency negative anomaly arises from the anticyclonic wave breaking over western North America (Fig. 5a). Also, because the model results of this study show that both NAO phases are preceded by high-frequency, synoptic-scale wave trains, the results of Feldstein (2003), together with those of this study, imply that the formation of the positive NAO phase is preceded by both high- and low-frequency wave trains, whereas that of the negative NAO phase is associated solely with a high-frequency wave train.

b. Sensitivity to the initial perturbations

As alluded to by Fig. 4, the above control runs demonstrate the sensitivity of the wave breaking character-

istics to the latitude of the initial perturbations. This result raises further questions.

- 1) Do the breaking waves correspond to NAO-like dipole patterns?
- 2) How sensitive are the results to the longitude and latitude of the initial perturbation?
- 3) Does the wave breaking in the NAO region always yield either one of the two NAO phases, and how abrupt is the transition between the two phases as the latitude of the base point increases?
- 4) How sensitive are the results to the sign and amplitude of the initial disturbance?

These four issues are addressed with the following calculations.

- 1) To determine if the breaking waves in the control runs correspond to NAO-like dipole patterns, the anomalous 300-hPa streamfunction is calculated. Meridional dipole patterns in the NAO region are found (Fig. 7), indicating that the wave breaking features of the life cycle calculations represent NAO-like patterns to a reasonable accuracy. However, as will be discussed in more detail below, Fig. 7 shows streamfunction anomalies with a large amplitude outside the NAO region.
- 2) To examine this issue, a series of life cycle calculations is carried out in a domain with the base point of the regressed initial perturbations located between 26° and 64°N and between 150° and 120°W. This domain is divided into two regions, one at lower latitudes, between 26°–35°N and 150°–120°W, and the other at higher latitudes, between 55°–64°N and 150°–120°W. Life cycle calculations are performed for 35 different base points for each region. From these 35 experiments, composites are derived by averaging over the individual experiments when the kinetic energy reaches its maximum. For the lower-latitude region, each member of the composite shows the same anticyclonic wave breaking characteristics as for the positive NAO phase illustrated in Fig. 2a. Similarly, for the higher latitude region, each member of the composite exhibits cyclonic wave breaking that resembles the negative NAO phase composite of Fig. 2b. This can be seen from the composite average anomalous streamfunction field (Fig. 8); the composite average fields for both the low- and high-latitude regions (see Figs. 8a and 8b, respectively) qualitatively resemble their observed counterparts (see Figs. 2c,d), with centers of action over Iceland and the midlatitude North Atlantic. As expected for such simple model experiments, there are also differences with the observed NAO structure. Particularly, the positive model NAO phase shows a weaker negative anomaly than that in observations. For the negative phase, the location of the negative center is too far upstream and is also weaker in comparison with the observations. This suggests that the initial

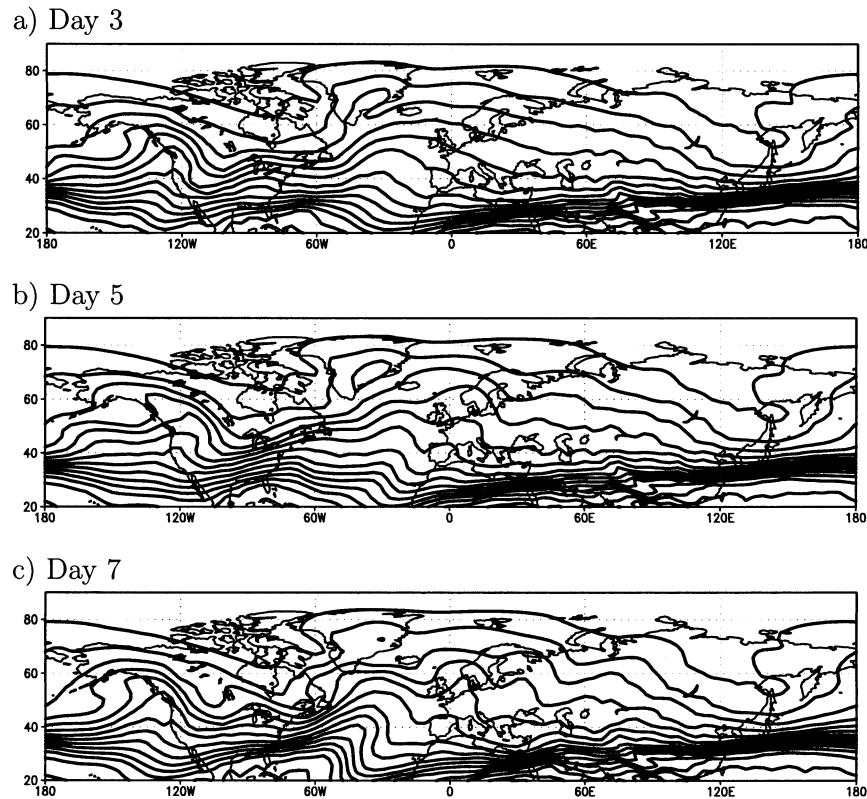


FIG. 5. Potential temperature on the 2-PVU surface for the initial perturbation at 30°N , 150°W : (a) day 3, (b) day 5, (c) day 7, (d) day 9, (e) day 10, and (f) day 11 (contour interval is 5.0 K).

value experiments capture the essential NAO-generating wave breaking process but may miss other aspects of the NAO evolution.

In contrast to the robust dipole response within the North Atlantic, responses with sizeable amplitudes, exhibiting much case-to-case variability are found at other locations throughout the Northern Hemisphere. This can be seen by comparing Figs. 7a,b with their respective composite mean fields (Figs. 8a,b). In the latter fields, signals outside the NAO region are much weaker than those shown in Fig. 7. To the extent that the above model results simulate the observed NAO, these results suggest that individual NAO life cycles do not resemble the composite NAO. Rather, these results suggest that the observed NAO represents an average of different NAO life cycles for which similar spatial patterns always occur only within the NAO region.

Experiments are also performed with initial perturbations both upstream (150°E – 150°W) and downstream (120°W – 30°E) of the above 150° – 120°W domain. The initial perturbations located upstream break before they reach the west coast of the United States; they do not reach the NAO region. The initial perturbations located farther downstream propagate through the NAO region into Europe and Asia where

they break. In summary, none of these calculations yielded NAO-like anomalies over the North Atlantic.

- 3) Simulations are performed with the initial perturbations located within the area between 36° – 54°N and 150° – 120°W , a range of latitudes in between those used to obtain Figs. 8a and 8b. The results do not show the above wave breaking characteristics, and therefore do not characterize either of the NAO phases. The evolved flow looks more like a wave train starting near the pole, traveling over the North Atlantic before describing an arc into the subtropics (Fig. 8c). This pattern resembles the wave packets in a barotropic model study by Lee (2000), for an initial wave packet centered at 45°N , 45°W . As the domain of the initial perturbations moves farther poleward a gradual transition to the negative phase takes place.
- 4) The sensitivity of the sign of the initial perturbation is also examined. For each case, qualitatively similar wave breaking characteristics were obtained. Therefore, the results are insensitive to the sign of the initial perturbation. The sensitivity of the amplitude of the initial perturbation is also examined. When the initial perturbation amplitude is increased by up to a factor of 10, the wave breaking characteristics

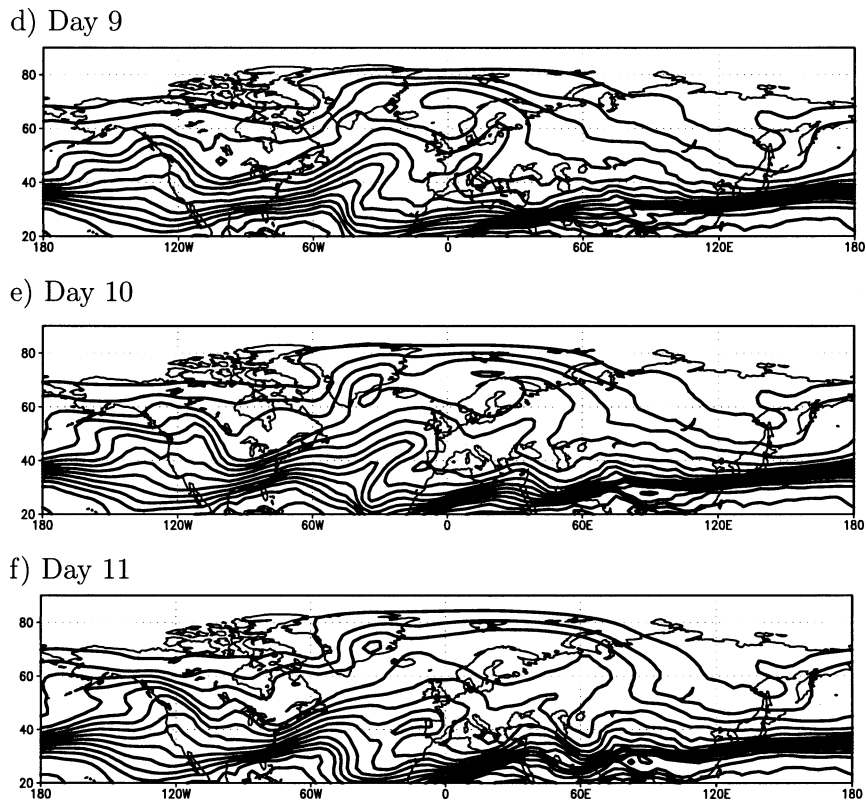


FIG. 5. (Continued)

remain qualitatively very similar. The primary differences are in the detailed spatial structure of the breaking waves and that the wave breaking occurs up to 2 days earlier with the larger amplitude. Furthermore, normal modes as initial disturbances have been tested. The corresponding experiments do not lead to NAO-like patterns.

The above results show that life cycle simulations with an appropriately located initial perturbation and with the observed three-dimensional climatological winter flow as a basic state are able to reproduce the spatial structure of both NAO phases with reasonable accuracy. Also, as shown in the calculations corresponding to question 2, these results are in broad agreement with the observed storm track changes over the Pacific Ocean (Fig. 4).

c. Sensitivity to the basic state

Calculations are performed using basic states centered around the onset day of either phase of the NAO. The results are qualitatively similar to those of the control case, when the initial perturbation at 30°N (60°N) is used for the positive (negative) phase. This, of course, is not surprising, since the NAO pattern is already present in the basic state. However, for basic states of up to 3 days before onset, initial perturbations located at

30°N (60°N) for the negative (positive) phase do not lead to the positive (negative) phase. In other words, it is not possible to reverse the phase of the NAO-like pattern by using the positive (negative) phase of the NAO as a basic state with the initial perturbation at 60°N (30°N). Instead, the resulting patterns do not resemble either phase of the NAO (not shown).

d. Sensitivity to surface friction

As the positive NAO phase corresponds to an enhanced jet and previous modeling studies (e.g., James and Gray 1986) have shown that the strength of the barotropic component of the flow generated by eddy life cycles depends on how strong is the surface friction, additional sensitivity experiments with surface friction included have been carried out. As stated in section 2a, sensitivity experiments are performed with the value of the surface damping time scale at 0.5, 1, and 2 days. These sensitivity experiments show results that are qualitatively similar to those of the inviscid experiments described above. While the wave amplitude decreases as the surface friction increases, the essential wave breaking characteristics are captured for both phases, as can be seen from Fig. 9 for the experiments with a 1-day damping time scale.

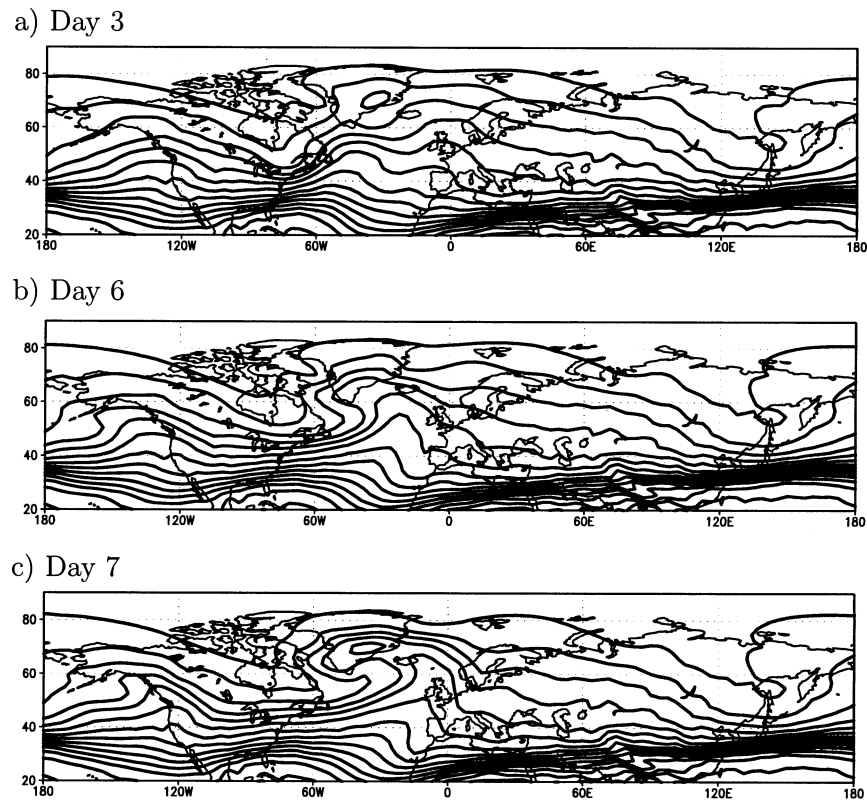


FIG. 6. Potential temperature on the 2-PVU surface for the initial perturbation at 60°N, 150°W: (a) day 3, (b) day 6, (c) day 7, (d) day 8, and (e) day 9 (contour interval is 5.0 K).

e. Time scale

To estimate if these experiments also reproduce the intrinsic time scale of the NAO, the e -folding time is calculated. For this purpose, the respective NAO-like streamfunction pattern (Figs. 8a,b) is projected onto the instantaneous streamfunction of each life cycle experiment. The projection time series are shown in Figs. 10a and 10b. For both phases, the average projection reaches its maxima near day 8 or 9 and decays afterward. Another interesting point is that the case-to-case variability for the negative phase is greater than that for the positive phase. An investigation of observational data shows qualitatively similar behavior (to be reported elsewhere). From these time series, the lag autocorrelation is calculated and the e -folding time scale is determined. The calculation yields an e -folding time scale of about 6 days, somewhat shorter than the 9 days found by Feldstein (2003) for the observed composite NAO life cycle (see Figs. 6 and 7 of that study). This could be due to the lack of consecutive wave breaking events in our life cycle simulations, which as shown by BLF, prolong the persistence of the NAO.

5. Zonally symmetric basic state

To analyze the extent to which the zonal asymmetries of the background flow are crucial for the two distinct

wave breakings associated with either phase of the NAO, additional experiments with zonally symmetric basic states have been carried out. The two sets of the experiments use various partial zonal-mean (an average over a limited range of longitudes) flows as a basic state and (a) normal mode and (b) finite amplitude initial perturbations. The basic states include climatological flows as well as composite flows taken from times prior to the onset of both NAO phases. (See Fig. 11 for a few selected basic states.)

a. Normal mode perturbation

The experiment for the climatological partial zonal average between 130° and 80°W (Fig. 11a) and a normal mode zonal wavenumber-6 initial perturbation shows a SE–NW tilt and a disturbance that breaks cyclonically. While the sense of the wave breaking corresponds to the tilt for the negative phase and this wave breaking occurs poleward of the basic state jet, the spatial scale is too small and the breaking occurs about 15° equatorward of the observed wave breaking (not shown). In the experiment for the climatological partial zonal average between 80° and 30°W (Fig. 11b) and a normal mode zonal wavenumber-6 initial perturbation, the tilt of the breaking wave is SW–NE, and the wave breaks anticyclonically on the equatorward side of the basic

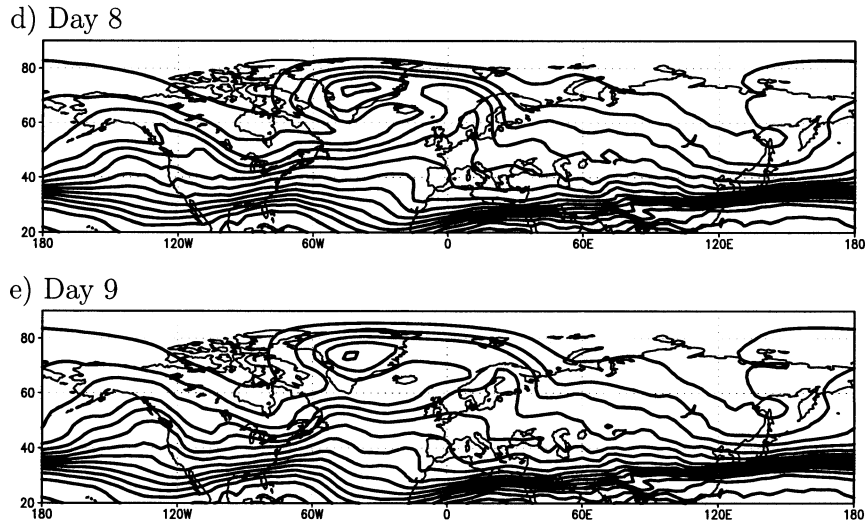


FIG. 6. (Continued)

state jet (not shown). The spatial scale is again too small. Also, the time scale for the evolution of these life cycle experiments is too short compared with the observed NAO.

The differences between these two experiments can be explained by the different meridional shear of the basic states between the latitudes of 20° and 50° N. The shear is cyclonic (anticyclonic) for the partial zonal average of 130° – 80° W (80° – 30° W). Therefore, the waves break according to the meridional shear. Similar results have been reported by Thorncroft et al. (1993).

Qualitatively similar results are retained by using partial zonal averages, such as 120° – 60° W, 60° W– 0° , and 90° W– 0° , as basic states and zonal wavenumbers 7 and 8 as initial perturbations. Using lag composites prior to the NAO onset as basic states (see Figs. 11c,d) does not

lead to an improvement of the results. Therefore, the results suggest that the essence of NAO growth cannot be represented by normal mode growth on a zonally symmetric background flow.

b. Finite-amplitude perturbation

To test the extent to which the structure of the initial perturbation affects the evolution of the baroclinic waves, we follow the same approach as in the previous section and use regressed finite amplitude perturbations derived from the observations.

In Figs. 12a, and 12b, snapshots of θ on the 2-PVU surface are shown for initial perturbations with base points at 30° N, 150° W and 60° N, 150° W, and the basic state averaged between 130° and 80° W (Fig. 11a). The

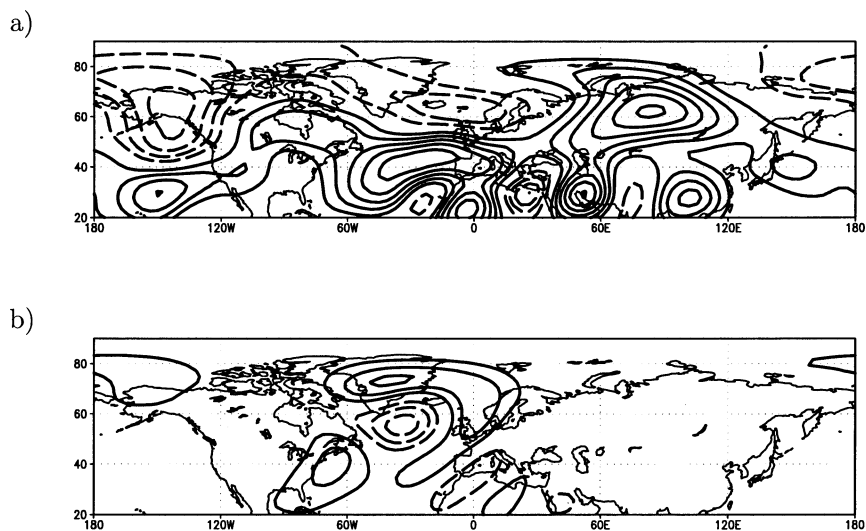


FIG. 7. Anomalous 300-hPa streamfunction for (a) initial perturbation at 30° N, 150° W, and (b) initial perturbation at 60° N, 150° W (contour interval is $2 \times 10^6 \text{ m}^2 \text{ s}^{-1}$).

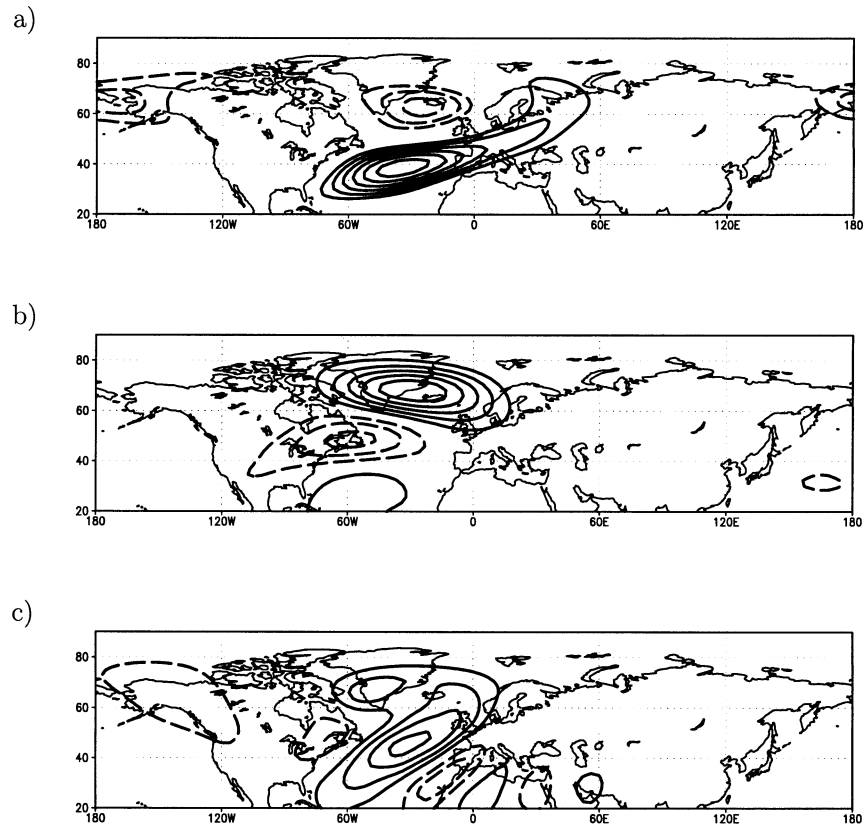


FIG. 8. Ensemble average of the anomalous 300-hPa streamfunction with initial perturbation locations in the domain (a) 26–35°N, 120°–150°W; (b) 55°–64°N, 120°–150°W, and (c) 36°–54°N, 120°–150°W (contour interval is $2 \times 10^6 \text{ m}^2 \text{ s}^{-1}$).

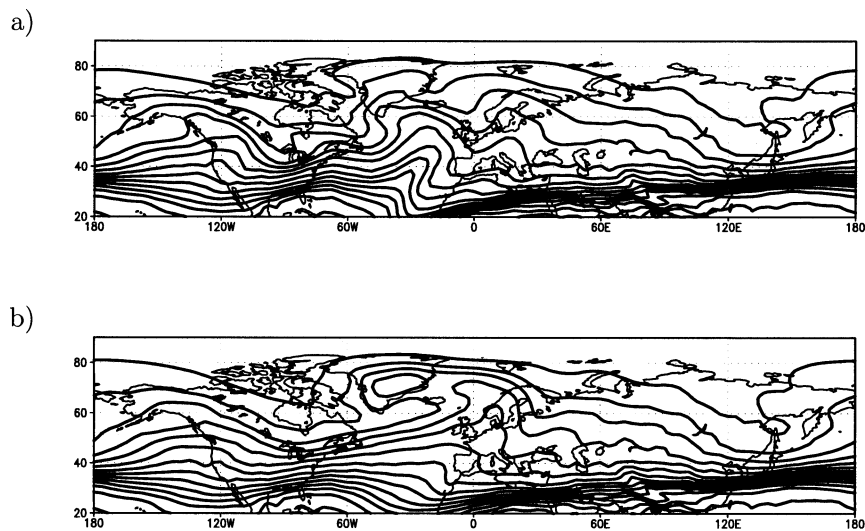
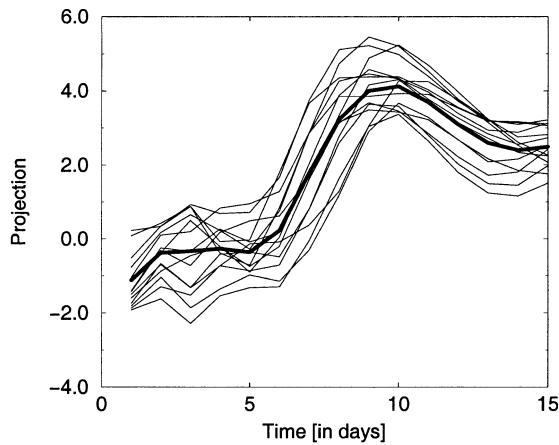


FIG. 9. Experiments with surface friction (damping time scale is 1 day): potential temperature on the 2-PVU surface for the initial perturbation at (a) 30°N, 150°W (day 7) and (b) 60°N, 150°W (day 8). Contour interval is 5.0 K.

a)



b)

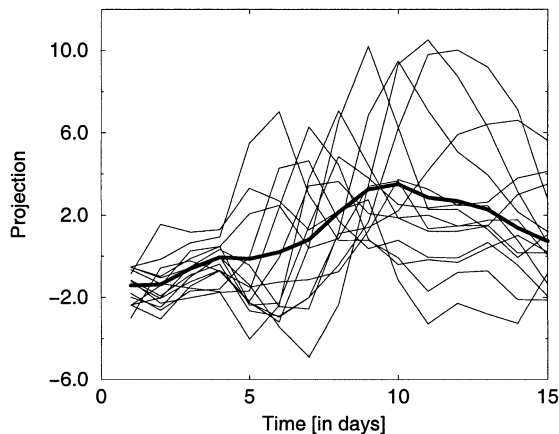


FIG. 10. Projection of the ensemble anomalous 300-hPa streamfunction with initial perturbation locations in the domain (a) 26° – 35° N, 120° – 150° W, and (b) 55° – 64° N, 120° – 150° W onto the instantaneous anomalous 300-hPa streamfunction field. The thick line indicates the mean of the individual projections (thin lines).

θ field shown corresponds to the time when the waves reach their maximal amplitude. The evolution for the initial perturbation at 30° N does not indicate wave breaking, rather there is development into omega-like structures with a slight SE–NW tilt (Fig. 12a). For the initial perturbation at 60° N, omega-like structures also emerge on the equatorward side of the basic-state jet. Farther poleward, an anomaly develops with SE–NW tilt and slight wave breaking (Fig. 12b). In the two cases for the basic state averaged over the region 80° – 30° W (Fig. 11b) with initial perturbations located at 30° N, 150° W and 60° N, 150° W, the perturbations again evolves into structures that do not exhibit the wave breaking characteristics of either NAO phase (Figs.

12c,d). These structures are in stark contrast with those illustrated in Figs. 5 and 6.

In summary, none of the experiments with a zonally symmetric basic state showed realistic wave breaking characteristics. This is in contrast to the experiments with a zonally asymmetric basic state, where the individual life cycle experiments showed the wave breaking characteristics of the NAO. These results suggest that zonal asymmetries in the basic state are crucial for the growth of the NAO.

6. Summary and conclusions

This study shows with a multilevel primitive equation model that when the three-dimensional NH climatological winter flow is used as a basic state, initially localized synoptic-scale waves undergo wave breaking during their evolution into NAO-like anomalies. The NAO is essentially the remnant of these breaking waves. As to be expected for such simple model experiments, there are also differences with the observed NAO structure, suggesting that the model experiments miss some aspects of the NAO life cycle.

The life cycle experiments show that the phase of the NAO depends on the latitudinal location of the initial perturbation over the Pacific Ocean 150° – 120° W. The positive phase is initiated by a perturbation located at relatively low latitudes 26° – 35° N and involves anticyclonic wave breaking along a SW–NE axis, occurring both along the west coast of North America and over the midlatitude and subtropical North Atlantic. The negative phase is triggered by an initial perturbation placed at relatively high latitudes 55° – 64° N and involves cyclonic wave breaking along a SE–NW axis, occurring on the poleward side of the climatological jet. This is consistent with the observations, which show that the Pacific storm track is displaced equatorward (poleward) prior to the onset of the positive (negative) NAO phase.

Results of this study suggest a much simpler picture for the evolution of the negative NAO phase. As described above, and as shown in the observational study of BLE, the negative NAO phase arises from a single cyclonic wave breaking, whereas the positive NAO phase originates from two separate anticyclonic wave breakings. For the negative phase, the single cyclonic wave breaking accounts for both centers of the NAO dipole. In contrast, for the positive phase, the negative center arises from the upstream anticyclonic wave breaking near the North American west coast, followed by eastward propagation of this negative center. The positive center derives from the much farther downstream anticyclonic wave breaking over the North Atlantic.

The above model results, thus, do not only produce NAO-like anomalies, but they also mimic the key wave breaking features found in the observations (BLF). To the extent that the low-frequency anomalies are a remnant of the wave breaking, this difference between the

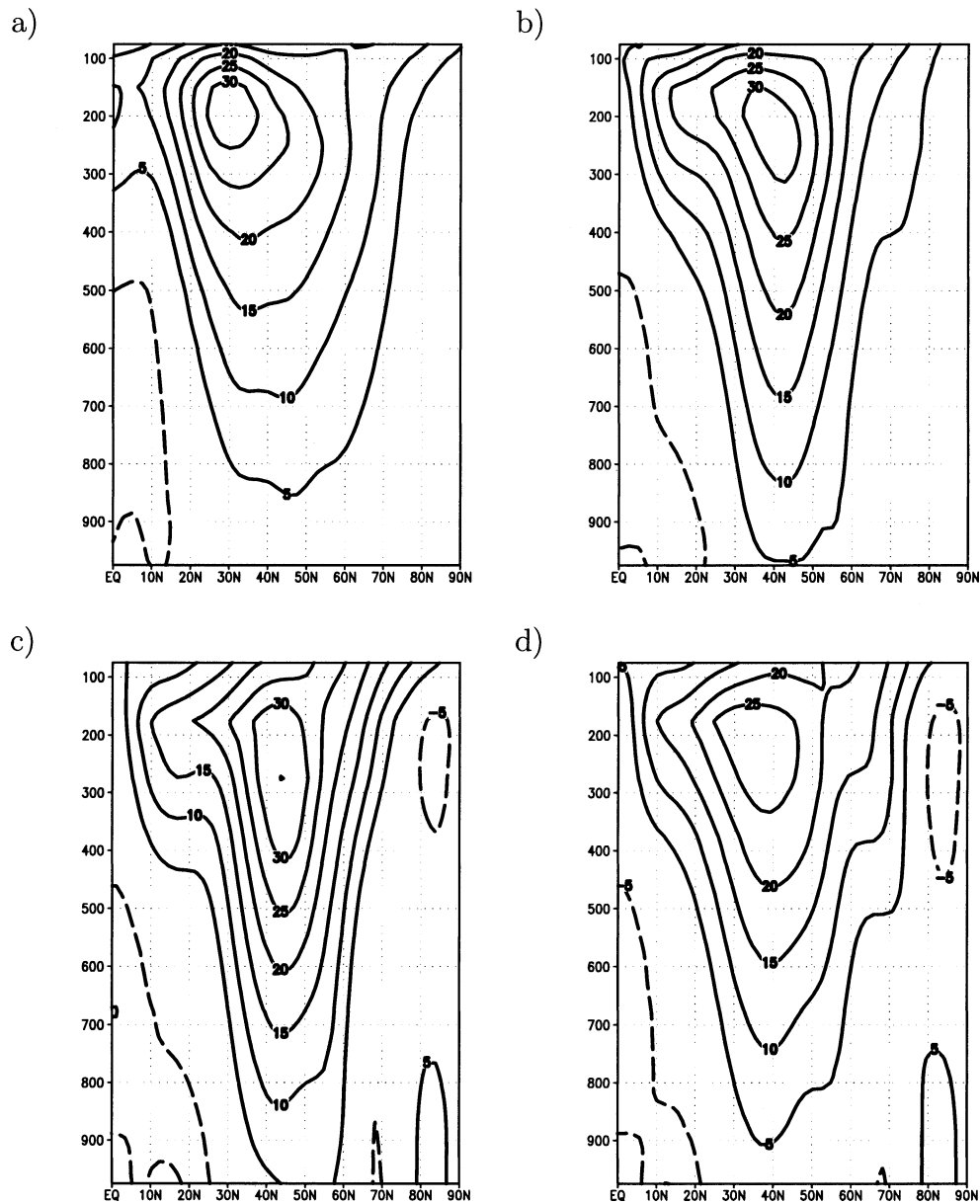


FIG. 11. Zonal mean zonal wind basic states (contour interval is 5 m s^{-1} , negative values are dashed, the zero line is omitted): (a) time-mean partial zonal average between 130° – 80° W; (b) time-mean partial zonal average between 80° – 30° W; (c) day -3 of the positive NAO phase, partial zonal average between 80° – 30° W; and (d) day -3 of the negative NAO phase, partial zonal average between 80° – 30° W.

two phases of the NAO is indeed consistent with the finding of Feldstein (2003) that the negative phase arises from in situ development, while the development of the positive phase is preceded by an upstream low-frequency wave train; only a single wave breaking is necessary for the in situ development of the negative-phase low-frequency anomaly, but more than one wave breaking is necessary for the formation of the positive-phase low-frequency wave train. For the positive phase, since the upstream wave breaking precedes the downstream wave breaking in the initial value calculations, these

two wave breakings are likely to be linked through downstream development.

The wave breakings that describe both phases of the NAO take place in the northeast Pacific and the North Atlantic, regions where the climatological flow is characterized by a weak meridional potential vorticity gradient and a strong stretching deformation. As large particle displacements tend to occur in flows with these properties, it is perhaps not surprising that the wave breaking associated with both NAO phases takes place in these regions.

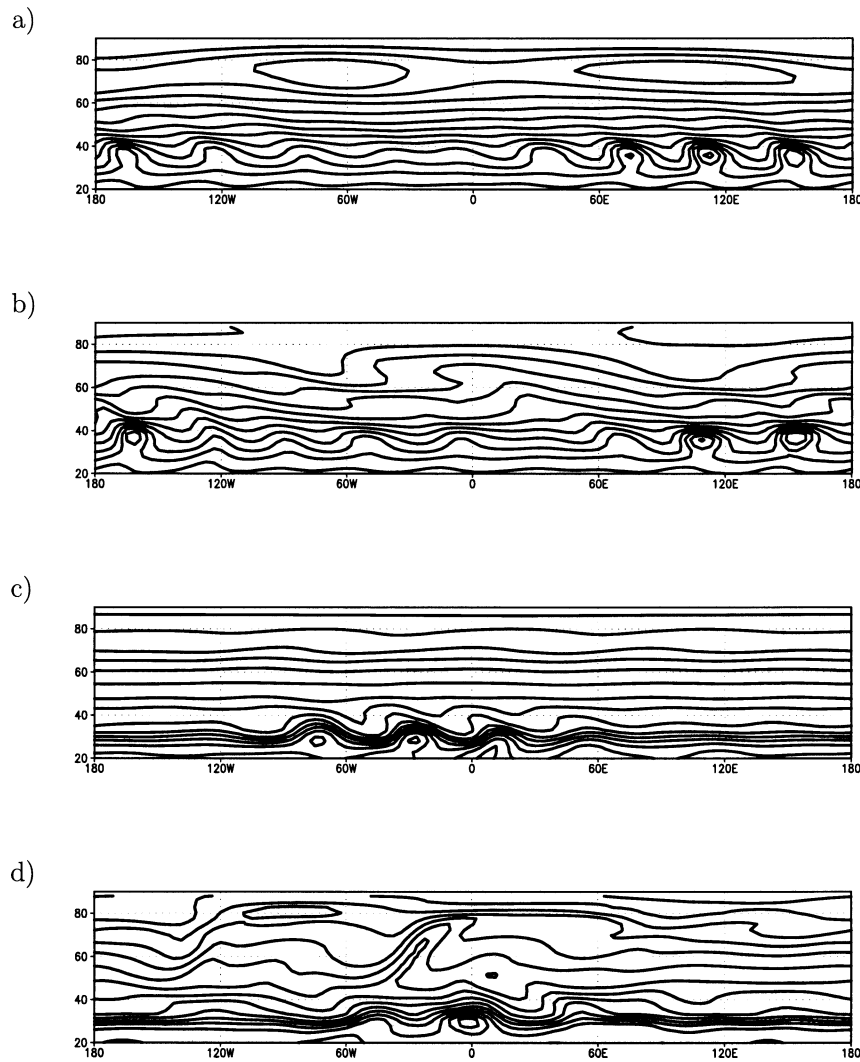


FIG. 12. Potential temperature on the 2-PVU surface for the basic-state partial zonal mean 130°–80°W (Nov–Mar) (a) initial perturbation at 30°N, 150°W, and (b) initial perturbation at 60°N, 150°W; for the basic-state partial zonal mean 80°–30°W (Nov–Mar) (c) initial perturbation at 30°N, 150°W, and (d) initial perturbation at 60°N, 150°W (contour interval is 5.0 K).

An ensemble of life cycle experiments consistently show dipole streamfunction anomalies in the NAO region, but with much case-to-case variability outside the NAO region. This implies that the NAO itself is not a solution of the equations; instead the NAO is the average of different individual solutions.

The set of experiments with zonally symmetric basic states fails to yield disturbances that resemble either phase of the NAO. These results lead to the conclusion that the zonally varying background flow is crucial for the correct spatial scale and sense of wave breaking for the observed NAO.

Feldstein (2003) finds an e -folding time scale for the decay of the composite NAO life cycle of about 9 days. The NAO lifecycle simulations presented in this study have an e -folding time scale of about 6 days. This difference could be due to the lack of consecutive wave

breaking events in the simulations. These subsequent wave breakings are by construction absent in our model calculations. BLF show that individual NAO events often involve a series of consecutive synoptic-scale wave breaking events. These consecutive wave breaking events are likely to prolong the persistence of the NAO. This result is consistent with the finding that transient eddy fluxes maintain low-frequency anomalies and also retard the propagation of Rossby waves (Robinson 1991; Branstator 1992).

Further studies are planned to closely examine the possible influence of a weak/strong stratospheric polar vortex on the breaking waves, and therefore the NAO. Such a connection, which has been proposed by Perlwitz and Graf (2001), Thompson et al. (2002), and Ambaum and Hoskins (2002), could have implications for predictability.

Acknowledgments. Thanks are due to Jim Benedict. We also thank two anonymous reviewers for their detailed and helpful comments on an earlier version of this manuscript. The research was funded by the National Science Foundation (ATM-0003039 and ATM-0001473). SL and SBF also acknowledge funding by the Deutsche Forschungsgemeinschaft (SFB 512) for a 4-week stay at the Universität Hamburg. We would like to thank the NOAA Climate Diagnostics Center for providing us with the NCEP–NCAR Reanalysis dataset.

REFERENCES

- Ambaum, M. H. P., and B. J. Hoskins, 2002: The NAO troposphere–stratosphere connection. *J. Climate*, **15**, 1969–1978.
- Benedict, J. J., S. Lee, and S. B. Feldstein, 2004: Synoptic view of the North Atlantic Oscillation. *J. Atmos. Sci.*, **61**, 121–144.
- Bjerknes, J., 1964: Atlantic air–sea interaction. *Advances in Geophysics*, Vol. 10, Academic Press, 1–82.
- Branscome, L. E., W. J. Gutowski Jr., and D. A. Stewart, 1989: Effect of surface fluxes on the nonlinear development of baroclinic waves. *J. Atmos. Sci.*, **46**, 460–475.
- Branstator, G. W., 1992: The maintenance of low-frequency anomalies. *J. Atmos. Sci.*, **49**, 1924–1945.
- Cai, M., and M. Mak, 1990: Symbiotic relation between planetary and synoptic-scale waves. *J. Atmos. Sci.*, **47**, 2953–2968.
- Cash, B. A., and S. Lee, 2001: Observed nonmodal growth of the Pacific–North American teleconnection pattern. *J. Climate*, **14**, 1017–1028.
- Chang, E. K. M., 1993: Downstream development of baroclinic waves as inferred from regression analysis. *J. Atmos. Sci.*, **50**, 2038–2053.
- Defant, A., 1924: Die Schwankungen der atmosphärischen Zirkulation über dem nordatlantischen Ozean im 25-jährigen Zeitraum 1881–1905. *Geogr. Ann.*, **6**, 13–41.
- Feldstein, S. B., 1994: A weakly nonlinear primitive equation baroclinic life cycle. *J. Atmos. Sci.*, **51**, 23–34.
- , 2002: Fundamental mechanisms of PNA growth and decay. *Quart. J. Roy. Meteor. Soc.*, **128**, 775–796.
- , 2003: The dynamics of NAO teleconnection pattern growth and decay. *Quart. J. Roy. Meteor. Soc.*, **129**, 901–924.
- Franzke, C., K. Fraedrich, and F. Lunkeit, 2001: Teleconnections and low-frequency variability in idealized experiments with two storm tracks. *Quart. J. Roy. Meteor. Soc.*, **127**, 1321–1339.
- Frederiksen, J. S., 1983: A unified three-dimensional instability theory of the onset of blocking and cyclogenesis. II: Teleconnection patterns. *J. Atmos. Sci.*, **40**, 2593–2609.
- Held, I. M., and M. J. Suarez, 1994: A proposal for the intercomparison of the dynamical cores of atmospheric general circulation models. *Bull. Amer. Meteor. Soc.*, **75**, 1825–1830.
- Higgins, R. W., and S. D. Schubert, 1993: Low-frequency synoptically active activity in the Pacific storm track. *J. Atmos. Sci.*, **50**, 1672–1690.
- Hoskins, B. J., and A. J. Simmons, 1975: A multi-layer spectral model and the semi-implicit method. *Quart. J. Roy. Meteor. Soc.*, **101**, 637–655.
- , and D. J. Karoly, 1981: The steady linear response of a spherical atmosphere to thermal and orographic forcing. *J. Atmos. Sci.*, **38**, 1179–1196.
- , M. E. McIntyre, and A. W. Robertson, 1985: On the use and significance of isentropic potential vorticity maps. *Quart. J. Roy. Meteor. Soc.*, **111**, 877–946.
- Hurrell, J. W., 1995: Decadal trends in the North Atlantic Oscillation: Regional temperatures and precipitation. *Science*, **269**, 676–679.
- James, I. N., and L. J. Gray, 1986: Concerning the effect of surface drag on the circulation of a baroclinic planetary atmosphere. *Quart. J. Roy. Meteor. Soc.*, **112**, 1231–1250.
- James, P. M., K. Fraedrich, and I. N. James, 1994: Wave–zonal-flow interaction and ultra-low-frequency variability in a simplified global circulation model. *Quart. J. Roy. Meteor. Soc.*, **120**, 1045–1067.
- Kim, H.-K., and S. Lee, 2001a: Hadley cell dynamics in a primitive equation model. Part I: Axisymmetric flow. *J. Atmos. Sci.*, **58**, 2845–2858.
- , and —, 2001b: Hadley cell dynamics in a primitive equation model. Part II: Non-axisymmetric flow. *J. Atmos. Sci.*, **58**, 2859–2871.
- Lau, N.-C., and M. J. Nath, 1991: Variability of the baroclinic and barotropic transient eddy forcing associated with monthly changes in the midlatitude storm tracks. *J. Atmos. Sci.*, **48**, 2589–2613.
- Lee, S., 2000: Barotropic effects on atmospheric storm tracks. *J. Atmos. Sci.*, **57**, 1420–1435.
- , and S. B. Feldstein, 1996: Two types of wave breaking in an aquaplanet GCM. *J. Atmos. Sci.*, **53**, 842–857.
- Marshall, J., and Coauthors, 2001: North Atlantic climate variability: Phenomena, impacts and mechanisms. *Int. J. Climatol.*, **21**, 1863–1898.
- Perlwitz, J., and H.-F. Graf, 2001: Troposphere–stratosphere dynamic coupling under strong and weak polar vortex conditions. *Geophys. Res. Lett.*, **28**, 271–274.
- Robinson, W. A., 1991: The dynamics of low-frequency variability in a simple model of the global atmosphere. *J. Atmos. Sci.*, **48**, 429–441.
- Sickmüller, M., R. Blender, and K. Fraedrich, 2000: Observed winter cyclone tracks in the Northern Hemisphere in re-analysed ECMWF data. *Quart. J. Roy. Meteor. Soc.*, **126**, 591–620.
- Simmons, A. J., J. M. Wallace, and G. W. Branstator, 1983: Barotropic wave propagation and instability, and atmospheric teleconnection patterns. *J. Atmos. Sci.*, **40**, 1363–1392.
- Thompson, D. W. J., M. P. Baldwin, and J. M. Wallace, 2002: Stratospheric connection to Northern Hemisphere wintertime weather: Implications for prediction. *J. Climate*, **15**, 1421–1428.
- Thorncroft, C. D., B. J. Hoskins, and M. E. McIntyre, 1993: Two paradigms of baroclinic-wave life-cycle behaviour. *Quart. J. Roy. Meteor. Soc.*, **119**, 17–55.
- Trenberth, K. E., G. W. Branstator, D. Karoly, A. Kumar, N.-C. Lau, and C. Ropelewski, 1998: Progress during TOGA in understanding and modeling global teleconnections associated with tropical sea surface temperatures. *J. Geophys. Res.*, **103**, 14 291–14 324.
- Vautard, R., and B. Legras, 1988: On the source of midlatitude low-frequency variability. Part II: Nonlinear equilibration of weather regimes. *J. Atmos. Sci.*, **45**, 2845–2867.
- Walker, G. T., and E. W. Bliss, 1932: World weather V. *Mem. Roy. Meteor. Soc.*, **4**, 53–83.
- Walther, G.-R., and Coauthors, 2002: Ecological responses to recent climate change. *Nature*, **416**, 389–395.